Rock and Soil Mechanics

Volume 44 | Issue 7 Article 7

11-3-2023

Simulation of seepage and heat transfer in 3D fractured rock mass based on fracture continuum method

Dong-dong LIU
School of Civil Engineering and Transportation, South China University of Technology, Guangzhou, Guangdong 510641, China; Guangzhou Municipal Engineering Design and Research Institute Co. Ltd., Guangzhou, Guangdong 510600, China, dond_liu@126.com

Li-xin WEI
Guangzhou Municipal Engineering Design and Research Institute Co. Ltd., Guangzhou, Guangdong 510600, China

Guo-yuan XU
School of Civil Engineering and Transportation, South China University of Technology, Guangzhou, Guangdong 510641, China

Yan-yong XIANG
School of Civil Engineering, Beijing Jiaotong University, Beijing 100044, China

Simulation of seepage and heat transfer in 3D fractured rock mass based on fracture continuum method

Abstract

The main challenge of simulating the processes of seepage and heat transfer in fractured rock mass is the heterogeneity of rock mass at various scales. In order to balance the efficiency and accuracy of numerical simulation, the two-dimensional fracture continuum method is extended to a three-dimensional one. Based on the depth-first search algorithm, the effective fractures contributing to the permeability of rock blocks are collected. The block permeability tensor is obtained by considering the contribution of effective fractures and rock matrix. The finite element software COMSOL Multiphysics is integrated with Matlab to generate a three-dimensional fracture continuum model that contains multiple blocks with various permeabilities. The simulation results show that due to the combination between stochastic continuum model and discrete fracture model, the fracture continuum model can avoid the complexity of addressing fracture networks and consider the spatial variability of rock mass permeability, thus both the simulation efficiency and accuracy are balanced. As the order of magnitude for the ratio of rock matrix permeability to fracture permeability ranges from 10−4 to 10−6, the discharge calculation error of the effective fracture network model exceeds 5%.

Keywords

3D fractured rock mass, seepage, heat transfer, depth-first search, fracture continuum method

Rock and Soil Mechanics 2023 44(7): 2143−2150 ISSN 1000−7598
https: //doi.org/10.16285/j.rsm.2022.6230 http://rocksoilmech.researchcommons.org/journal

Simulation of seepage and heat transfer in 3D fractured rock mass based on fracture continuum method

LIU Dong-dong[1, 2], WEI Li-xin[2], XU Guo-yuan[1], XIANG Yan-yong[3]

1. School of Civil Engineering and Transportation, South China University of Technology, Guangzhou, Guangdong 510641, China
2. Guangzhou Municipal Engineering Design and Research Institute Co. Ltd., Guangzhou, Guangdong 510600, China
3. School of Civil Engineering, Beijing Jiaotong University, Beijing 100044, China

Abstract: The main challenge of simulating the processes of seepage and heat transfer in fractured rock mass is the heterogeneity of rock mass at various scales. In order to balance the efficiency and accuracy of numerical simulation, the two-dimensional fracture continuum method is extended to a three-dimensional one. Based on the depth-first search algorithm, the effective fractures contributing to the permeability of rock blocks are collected. The block permeability tensor is obtained by considering the contribution of effective fractures and rock matrix. The finite element software COMSOL Multiphysics is integrated with Matlab to generate a three-dimensional fracture continuum model that contains multiple blocks with various permeabilities. The simulation results show that due to the combination between stochastic continuum model and discrete fracture model, the fracture continuum model can avoid the complexity of addressing fracture networks and consider the spatial variability of rock mass permeability, thus both the simulation efficiency and accuracy are balanced. As the order of magnitude for the ratio of rock matrix permeability to fracture permeability ranges from 10^{-4} to 10^{-6}, the discharge calculation error of the effective fracture network model exceeds 5%.

Keywords: 3D fractured rock mass; seepage; heat transfer; depth-first search; fracture continuum method

1 Introduction

The analysis of geothermal mining system is based on the conceptual models, including equivalent porosity model(EPM)[1], double porosity model (DPM)[2], discrete fracture network (DFN) model[3], stochastic continuum model(SCM)[4], fracture continuum model(FCM)[5] and lattice Boltzmann model(LBM)[6]. In addition to the use of the principles of mechanics, the conceptual model establishment also requires reasoning and estimation based on the judgment of the research object[7]. Considering different research purposes, Assteerawatt[8] classified the problems in time and space domains, and proposed the corresponding multi-scale models.

The thermal reservoir of enhanced geothermal systems generally contains complex fracture networks, and the fracture network tends to cause the heterogeneous permeability distribution in the rock mass[9−11]. There are great defects on the existing reservoir-scale numerical models, e.g. the EPM ignores the disconnection between the fractures and overestimates the equivalent reservoir permeability; the DFN is apt to generate low-quality elements and reduce the computational efficiency and accuracy; and the SCM ignores the fracture statistical characteristics of the dip angle, dip direction, trace length and aperture due to the assumption on the randomly distributed permeability. By combining the DFN and SCM, the FCM can avoid the complex treatment on the stochastic fracture network, and can consider the heterogeneous permeability distribution of the thermal reservoir caused by fractures. The permeabilities of rock matrix and fracture are superimposed to obtain the equivalent permeability of grid blocks in the FCM. El et al.[12], Vu et al.[13], Hadgu et al.[14], Hartley and Joyce[15], Sweetenham et al.[16], Sandve et al.[17] and Chen et al.[18] simulated the three-dimensional (3D) seepage in fractured rock mass by using the FCM, but directly summed the contribution of all fractures without considering the grid block connectivity, and overestimated the equivalent permeability. Luo[19] utilized the depth-first search (DFS) algorithm to judge the connectivity of grid blocks, neglected the fractures with little contribution to the grid block connectivity, and developed a two-dimensional (2D) FCM but not a 3D one. Therefore, it is necessary to carry out research on the FCM for the 3D seepage and heat transfer processes to improve the calculation accuracy.

In this paper, the method of extracting the effective DFN from a 3D fractured rock mass is firstly introduced to eliminate the isolated fractures (groups) with little contribution to seepage, and the concept of single fracture permeability tensor is described. Then the FCM of the DFN is expounded. Since the direct or indirect connectivity between fractures and grid blocks is not considered in the conventional FCM, the DFS algorithm is used to judge the grid block connectivity in order to appropriately avoid exaggerating the grid block permeability, and to investigate the FCM applicability for the fractured rock mass with nonnegligible rock matrix permeability.

Received: 8 August 2022 Accepted: 15 November 2022
First author: LIU Dong-dong, male, born in 1992, PhD candidate, focusing on multiphysics couplings in porous media. E-mail: dond_liu@126.com

2 Effective DFN for fractured rock mass

2.1 Identification of seepage path

In the equivalent stochastic DFN, directly summing the fracture permeabilities may overestimate the permeability of grid blocks. For the two close-spaced disconnected fractures in the fractured rock model, these two fractures are esteemed to be connected if they are covered by the same grid block in the FCM. In order to eliminate this interference, it is necessary to judge the connectivity between fractures and grid blocks. Here, the following method is adopted. The x direction is taken as an example. If a group of connected fractures cannot penetrate the left and right boundaries, the group of connected fractures are not considered to contribute to the permeability in the x direction, such as the 2D DFN presented in Fig. 1. In Fig. 1, points A and C are the intersections of fractures AB and BC with the left boundary of the grid block, respectively; points D and F are the intersections of fractures DE and EF with the right boundary of the grid block, respectively; fracture AB intersects with fracture BC at point B; and fracture DE intersects with fracture EF at point E.

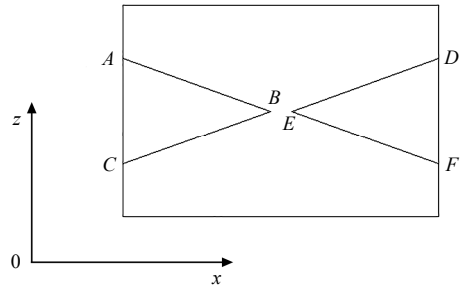

Fig. 1 Example of disconnected fracture networks

2.2 Effective DFN

In the fractured rock mass with low-permeability rock matrix, the fracture provides the main groundwater flow channel. The fracture that is directly or indirectly connected to the inlet and outlet boundaries plays a controlling role, i.e. the effective DFN. The effective DFN can remove isolated fractures (groups) that contribute little to seepage. The DFS algorithm is used to judge the connectivity between fractures and grid blocks to establish the effective DFN. The effective DFN model is generated from the original fractured rock model by DFS algorithm.

In Fig. 2, only the fractures connected with permeable boundaries are retained by using the DFS algorithm. The effective DFN is dominated by both of fracture connectivity and boundary hydraulic conditions. The pretreatment on fracture networks can effectively decrease the secondary fractures and provide the possibility of reducing the calculation amount on the simulation of seepage and heat transfer in fractured rock mass.

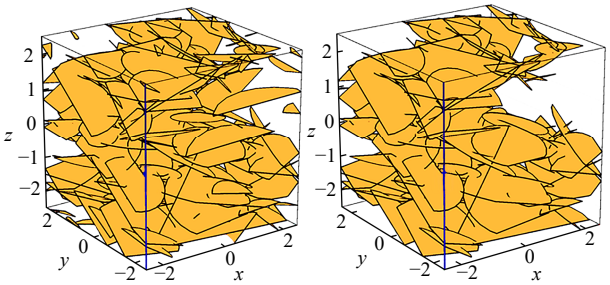

Fig. 2 Initial fracture model (left) and effective fracture network model (right) (m)

3 FCM for fractured rock mass

3.1 Equivalent permeability tensor of grid blocks

According to the Darcy's law, the fracture permeability in the direction parallel to the fracture wall is

$$\kappa = \frac{e^2}{12} \tag{1}$$

where κ is the fracture permeability in the direction parallel to the fracture wall; and e is the fracture hydraulic aperture.

In the 3D rectangular coordinate system, the fracture permeability tensor can be expressed by the cosine of the fracture normal direction as

$$\boldsymbol{\kappa}_{\mathrm{f}} = \kappa \begin{bmatrix} 1-n_x n_x & -n_x n_y & -n_x n_z \\ -n_y n_x & 1-n_y n_y & -n_y n_z \\ -n_z n_x & -n_x n_y & 1-n_z n_z \end{bmatrix} \tag{2}$$

where $\boldsymbol{\kappa}_{\mathrm{f}}$ is the fracture permeability tensor; n_x, n_y and n_z are the cosines of the angle between fracture normal direction and the x, y, z axes, respectively.

The fracture permeability tensor can also be expressed in terms of fracture orientation and dip direction as

$$\boldsymbol{\kappa}_{\mathrm{f}} = \kappa \begin{bmatrix} 1-\sin^2\omega\sin^2\gamma & \frac{1}{2}\sin 2\omega\sin^2\gamma & -\frac{1}{2}\sin\omega\sin 2\gamma \\ \frac{1}{2}\sin 2\omega\sin^2\gamma & 1-\cos^2\omega\sin^2\gamma & \frac{1}{2}\cos\omega\sin 2\gamma \\ -\frac{1}{2}\sin\omega\sin 2\gamma & \frac{1}{2}\cos\omega\sin 2\gamma & \sin^2\gamma \end{bmatrix} \tag{3}$$

where ω and γ are the dip direction and dip angle of the fracture, respectively.

Based on the principle of hydraulic equivalence, the contribution of a fracture to the grid block connected with this fracture permeability is

$$\boldsymbol{\kappa}_{\mathrm{c}} = \varphi_{\mathrm{f}} \boldsymbol{\kappa}_{\mathrm{f}} \tag{4}$$

where $\boldsymbol{\kappa}_{\mathrm{c}}$ is the contribution of a fracture to the permeability tensor of a grid block; $\varphi_{\mathrm{f}} = s_{\mathrm{e}} e / l^3$ is the proportion of fracture volume in a grid block, in which l is the side length of the grid block, and s_{e} is the fracture area in a

grid block.

By superimposing the permeability of rock matrix and contribution of each fracture, the equivalent permeability tensor of a grid block is

$$\boldsymbol{\kappa}_{\mathrm{e}}=\sum_{i=1}^{N}\varphi_{\mathrm{fi}}\boldsymbol{\kappa}_{\mathrm{c}i}+\left(1-\sum_{i=1}^{N}\varphi_{\mathrm{fi}}\right)\boldsymbol{\kappa}_{\mathrm{r}} \tag{5}$$

where $\boldsymbol{\kappa}_{\mathrm{r}}$ is the permeability tensor of rock matrix; i is the serial number of fracture passing through the grid block; and N is the number of fracture passing through the grid block.

In order to determine the permeability of a grid block, the stochastic fracture network is generalized into a disconnected graph according to the graph theory, and the DFS algorithm is used to identify the seepage path along the hydraulic pressure gradient direction. Before the calculation of the grid block permeability, the seepage path in the research domain needs to be searched. The search process is as follows: (1) determine the relative positional relationship of fractures in the research domain; (2) treat the permeable boundaries in the research domain as fractures and record the intersection relationships of fractures by the adjacency matrix; (3) eliminate the fracture that is not directly or indirectly connected to the inlet and outlet boundaries of the interest domain by traversing the adjacency matrix method[20]. After the seepage path search for the research domain, the equivalent permeability of grid blocks is calculated based on the effective DFN. The calculation process is as follows: (4) determine the relative positional relationship of fractures in grid blocks; (5) treat the permeable boundaries in the grid blocks as fractures and record the intersection relationships of fractures by the adjacency matrix method; (6) select the fractures directly or indirectly connected to at least two permeable boundaries of the grid block; (7) calculate the equivalent permeability of grid blocks by using Eq. (5); (8) loop the steps (4), (5), (6) and (7) until the equivalent permeability of all the grid blocks is calculated. The equivalent permeability of grid blocks is calculated by following the procedure presented in Fig. 3.

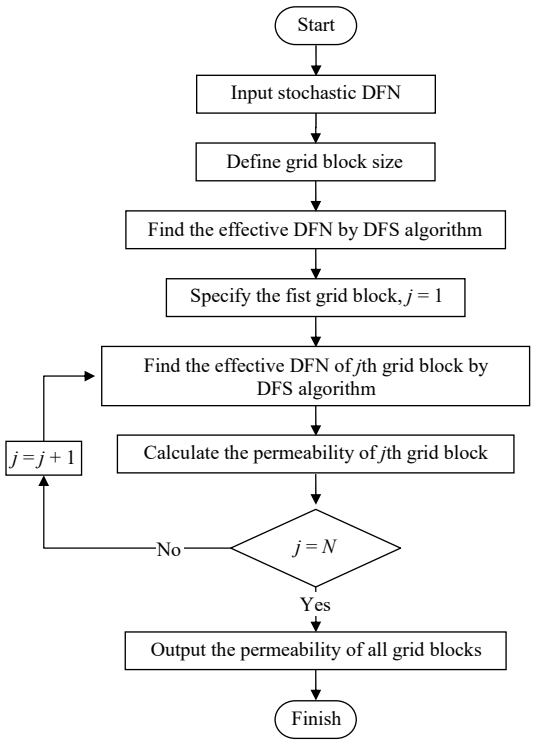

Fig. 3 Flowchart for calculating the permeability of grid blocks in fractured rocks

3.2 FCM verification by a single fractured rock mass

In order to verify the proposed FCM, the finite element software COMSOL Multiphysics combined with Matlab is applied to study the 3D seepage in a single fractured rock mass in terms of different fracture slopes and to compare the seepage flux of the FCM and DFN. Some assumptions are made as follows: the seepage follows the Darcy's law; the heat transfer between rock and fluid obeys instantaneous heat balance; the influence of temperature on the physical properties of rock and fluid is not considered. Without loss of generality, the fracture is rectangular, the fracture length along the orientation is fixed at 2 m, the projection length of the fracture along the dip direction on the horizontal plane is fixed at 20 m, the projection length of the fracture along the vertical direction varies in the range of 0−20 m, and the fracture dip angle changes within the range of $0^{\circ}-45^{\circ}$. For the single fractured rock mass models with different fracture dip angles presented in Fig. 4, the upper, lower, front and rear boundaries are set to be impermeable, and the left and right boundaries are set to be permeable, with a water pressure difference of 100 kPa. The rock matrix permeability is 3×10^{-15} m^2, and each fracture hydraulic aperture is 10^{-3} m. The side lengths of the grid block are selected as 0.5 m, 1 m and 2 m, respectively.

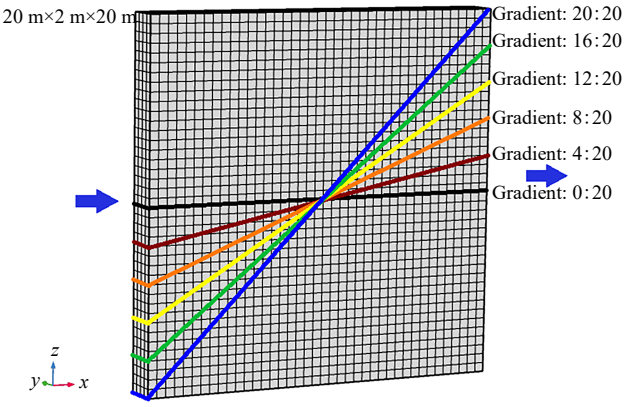

Fig. 4 Schematic diagram of fractures with different slope gradients

In Fig. 4, the inclined fracture may pass through the opposite two-side boundary, adjacent two-side boundary or adjacent three-side boundary of a grid block, resulting in great different seepage behaviors. In this paper, the grid blocks inserted by fractures are classified into two categories including the original grid block and modified grid block. Figure 5 shows a schematic diagram of these two different grid blocks.

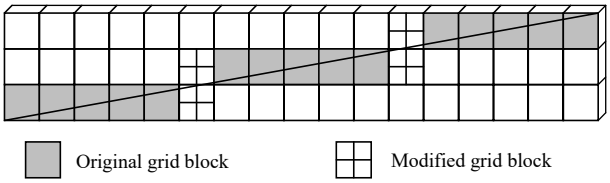

Fig. 5 Schematic diagram of two grid blocks

The identification of the two different grid blocks is based on the connectivity between the grid block boundaries. In this paper, the parallel boundaries are postulated to be the same boundary. As a result, a regular hexahedral grid block contains three types of boundaries. The specific criterion for judging the grid block type is: the number of the types of the connected boundaries in the original grid block is less than three, and that in the modified grid block is equal to three. If the permeability tensor of a grid block is calculated according to Eq. (2), the seepage of the original grid block and the modified grid block will be dominated by the same direction. However, the seepage paths in these two types of grid blocks are different in the FCM: the fluid in the modified grid block mainly flows in the normal direction of the unconnected boundaries in the original grid block, while the fluid in the original grid block mainly flows in the normal direction of the connected boundaries. In Fig. 5, the left and right boundaries are assumed to be permeable, and impermeable for other boundaries. The seepage in the original grid block mainly follows along the horizontal direction, while the seepage in the modified grid block mainly follows along the vertical direction. In order to match the seepage behaviors of the modified grid block, it is necessary to deal with the permeability of the modified grid block. Here, the following approach is adopted: the permeability of the modified grid block is calculated by using Eq. (2), and the maximum absolute value is selected as the permeability of the grid block in three directions. The advantage of the treatment is: in the corner of a grid block where the fractures pass through, the hydraulic pressure drop is so small that the larger permeability will not cause great deviation in the seepage flux and the accuracy of local seepage paths will be guaranteed.

Figure 6 depicts the spatial distribution of the permeability in x direction of the single fractured rock mass shown in Fig. 4. The smaller the size of the grid block, the closer the high permeability zone of the FCM to the plate fracture model, and vice versa. Table 1 lists the outflows from the right boundary in Fig. 5. The relative errors of the outflow from the FCM are within 5% for the grid block with the side length of 0.5 m.

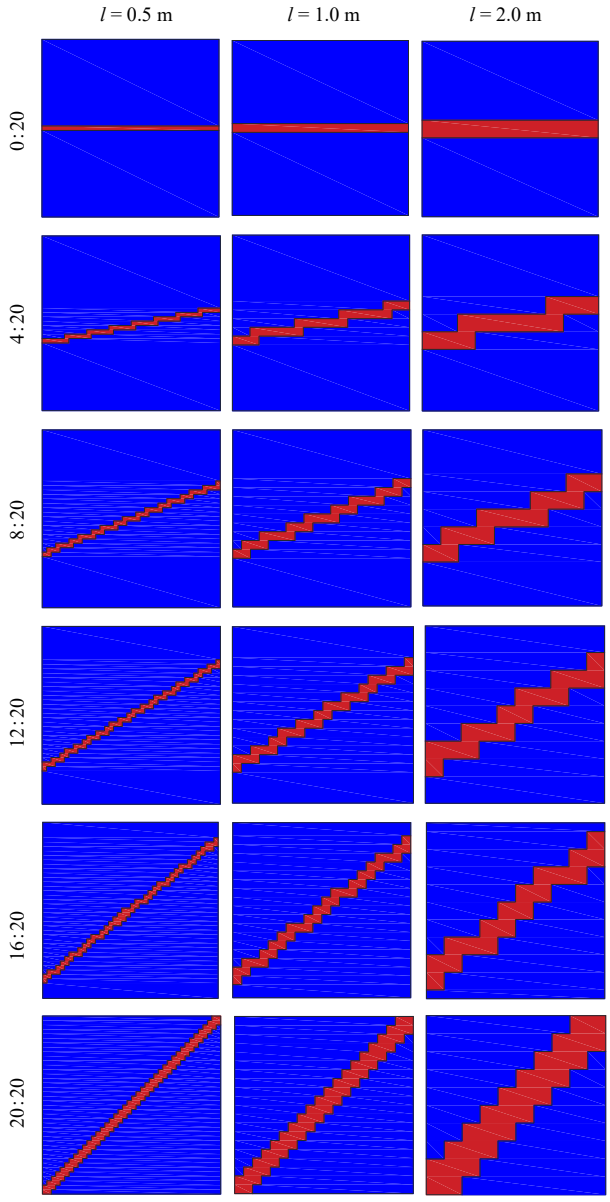

Fig. 6 Schematic diagrams of permeability in x-direction along vertical profile (blue: low-permeability zone; red: high-permeability zone)

4 Numerical simulation based on effective DFN model

The FCM is constructed based on the removal of isolated fractures (groups). Strong hydraulic connection between fractures and rock mass may exist for the rock matrix with nonnegligible permeability. It is necessary to explore the influences of eliminating isolated fractures

Table 1 Outflows in FCM and DFN model

Slope gradient of fracture	Outflow of DFN model /($m^3 \cdot s^{-1}$)	Outflow of FCM /($m^3 \cdot s^{-1}$)			Relative error /%		
		l = 0.5 m	l = 1.0 m	l = 2.0 m	l = 0.5 m	l = 1.0 m	l = 2.0 m
0:20	4.17×10^{-4}	4.22×10^{-4}	4.26×10^{-4}	4.44×10^{-4}	1.20	2.16	6.47
4:20	4.02×10^{-4}	4.10×10^{-4}	4.19×10^{-4}	4.39×10^{-4}	1.99	3.98	9.20
8:20	3.60×10^{-4}	3.72×10^{-4}	3.82×10^{-4}	4.04×10^{-4}	3.33	6.11	12.22
12:20	3.08×10^{-4}	3.20×10^{-4}	3.29×10^{-4}	3.54×10^{-4}	3.90	6.82	14.94
16:20	2.55×10^{-4}	2.66×10^{-4}	2.78×10^{-4}	3.04×10^{-4}	4.31	9.02	19.22
20:20	2.07×10^{-4}	2.17×10^{-4}	2.29×10^{-4}	2.59×10^{-4}	4.83	10.63	25.12

(groups) on the seepage flux and temperature field of fractured rock mass. The left model of fractured rock mass in Fig. 2 is taken as an example. The finite element software COMSOL Multiphysics combined with Matlab is used to investigate the differences of seepage, hydraulic pressure and temperature among fractured rock masse with different permeability ratios of rock matrix to fracture, e.g. 10^{-1}, 10^{-2}, 10^{-3}, 10^{-4}, 10^{-5}, 10^{-6}, 10^{-7}, 10^{-8} and 10^{-9}. For convenience, each fracture hydraulic aperture is assumed to be 60 μm.

4.1 Seepage simulation

Table 2 compares the outflows obtained from the original and effective DFNs. The outflow of effective DFN model is close to that of original DFN model for the fractured rock mass where the permeability differences between fracture and rock matrix are not great. It can be explained that the removed fractures can be equivalent to rock matrix with the same size and similar permeability. For the rock matrix permeability larger than the fracture permeability of 0.1%, the relative error of outflow between the original and effective DFN models is less than 3%. With the decrease of rock matrix permeability, the permeability of fractured rock mass is greatly reduced due to the eliminated fractures, and the relative error of outflow even exceeds 10%. For the low-permeable rock matrix, the fluid mainly flows in dominant fractures, and the effective DFN model becomes more accurate. In summary, the outflow accuracy estimated by the effective DFN model for the low- or high-permeable rock matrix can be guaranteed, while some attention needs to be paid to the calculation accuracy of the effective DFN model for the moderate-permeable rock matrix, e.g. the ratio of rock matrix permeability to fracture permeability is in the range of 10^{-4}–10^{-6}.

Table 2 Outflows in original and effective DFN models

κ_r/κ	Outflow of original DFN model /($m^3 \cdot s^{-1}$)	Outflow of effective DFN model /($m^3 \cdot s^{-1}$)	Relative error/%
10^{-1}	$1.501\ 0\times10^{-2}$	$1.500\ 8\times10^{-2}$	0.01
10^{-2}	$1.509\ 5\times10^{-3}$	$1.507\ 5\times10^{-3}$	0.13
10^{-3}	$1.588\ 1\times10^{-4}$	$1.569\ 5\times10^{-4}$	1.17
10^{-4}	$2.150\ 8\times10^{-5}$	$2.018\ 3\times10^{-5}$	6.16
10^{-5}	$4.892\ 6\times10^{-6}$	$4.319\ 2\times10^{-6}$	11.72
10^{-6}	$2.914\ 0\times10^{-6}$	$2.700\ 4\times10^{-6}$	7.33
10^{-7}	$2.540\ 3\times10^{-6}$	$2.439\ 2\times10^{-6}$	3.98
10^{-8}	$2.472\ 8\times10^{-6}$	$2.411\ 8\times10^{-6}$	2.47
10^{-9}	$2.469\ 0\times10^{-6}$	$2.409\ 0\times10^{-6}$	2.43

Figure 7 compares the hydraulic pressures in the original and effective DFN models. The hydraulic pressure in the two different DFNs is basically consistent in the case that the permeability differences between fractures and rock matrix are small. The channeling effects of fractures are insignificant due to the weak hydraulic connections between fractures and rock matrix. With the decrease of rock matrix permeability, the hydraulic pressure differences between the two different DFN models become large owing to the increasing hydraulic connections between fractures and rock matrix. However, the hydraulic pressure differences between the two different models are not great since the channeling effects of fractures are not strong. For the rock matrix with very low permeability, the hydraulic connections between fractures and rock matrix are weak, the channeling effects of fractures become more significant and result in more heterogeneous hydraulic pressure distribution in the research domain. As a result, great hydraulic pressure differences exist between the two different DFN models.

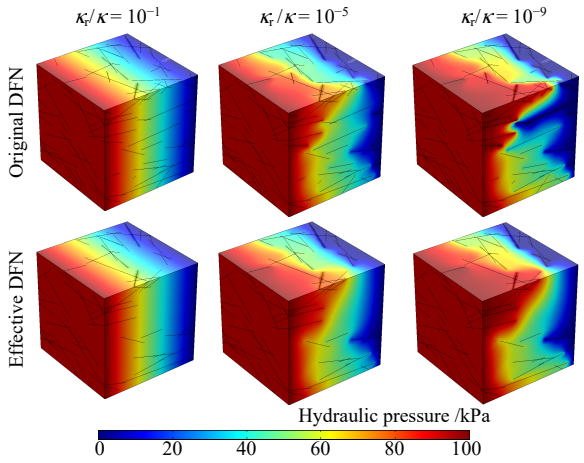

Fig. 7 Hydraulic pressures in original and effective DFN models

4.2 Seepage and heat transfer simulation

Figure 8 compares the temperature fields in the original and effective DFN models at 2×10^6 s. The low temperature range of the effective DFN model is smaller than that of

the original DFN model under the same working condition. The removed isolated fractures (groups) in the effective DFN model reduce the rock mass permeability so that less low-temperature water flows into the research domain from the left boundary and smaller low-temperature area appears. However, the isolated fractures (groups) have little effects on the temperature of fractured rock mass.

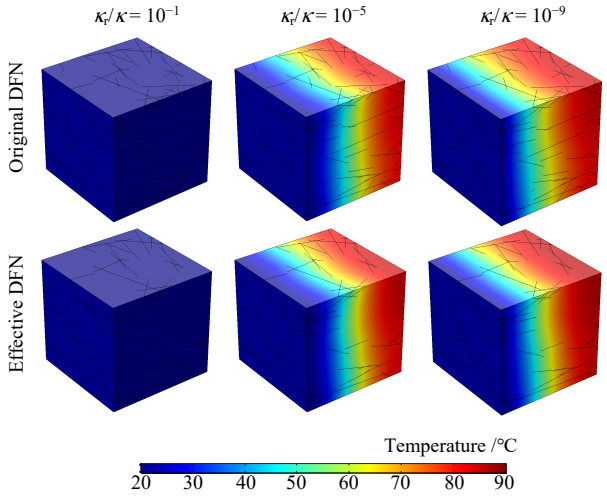

Fig. 8 Temperature fields in original and effective DFN models

5 Numerical simulation based on FCM

The FCM is used to simplify the original fractured rock mass. The finite element software COMSOL Multiphysics combined with Matlab is applied to investigate the differences of the seepage, hydraulic pressure and temperature field among the FCMs with the side lengths of grid block of 0 m (DFN model), 0.5 m and 1.0 m.

5.1 Seepage simulation

The rock matrix permeability and each fracture aperture are postulated to be 3×10^{-15} m^2 and 60 μm, respectively. Based on the outflow of the original DFN model, the relative errors of outflow obtained from FCMs with and without DFS algorithm are shown in Fig. 9. For FCMs with the same grid block, the outflow of the FCM with DFS algorithm is more accurate than that of the conventional FCM without DFS algorithm, i.e. the direct summation of fracture permeability exaggerates the permeability of grid blocks. For FCMs obtained by the same simplified method, the smaller the grid block size, the closer the outflow of the FCM to the original DFN model. The grid blocks of small size can fully reflect the spatial variability of the seepage channel in the original DFN model, while the grid blocks of large size cannot accurately capture the original seepage channels, resulting in the average between the connected and disconnected domains. Compared with the DFS algorithm, changing the grid block size can remarkably impact the seepage flux in the FCM. Therefore, the appropriate grid block size should be selected to ensure the FCM accuracy, and then the DFS algorithm should be adopted to improve the calculation accuracy of seepage flux.

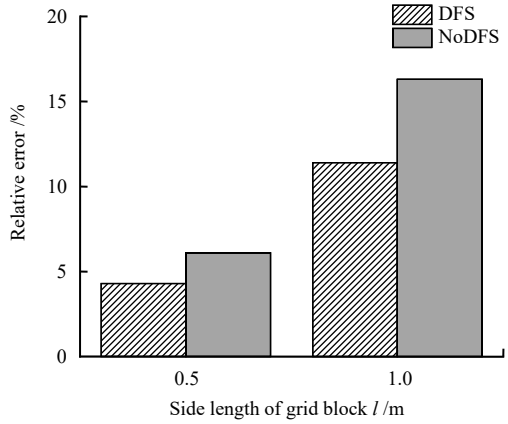

Fig. 9 Comparisons of relative errors of total outflow in FCMs

Figure 10 compares the hydraulic pressures in FCMs with and without DFS algorithm. The hydraulic pressure in the FCM with DFS algorithm is closer to that of the DFN model compared the FCM without DFS algorithm, especially the hydraulic pressure near the front and upper boundaries. It is verified that the FCM with DFS algorithm can give more accurate hydraulic pressure.

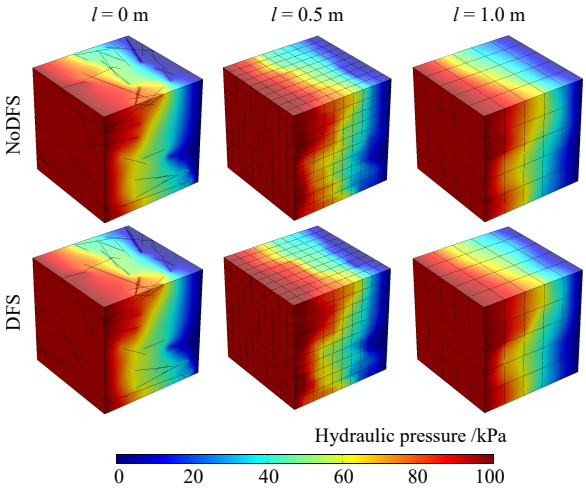

Fig. 10 Hydraulic pressures in FCMs with and without DFS algorithm

Figure 11 compares the permeability distributions in FCMs with and without DFS algorithm. The grid block permeability obtained by these two methods is the same in most domains (sparse fracture area and fracture connected area), while the permeability of grid blocks without DFS algorithm is two orders of magnitude larger than that of grid blocks with DFS algorithm (fracture disconnected area). The conventional FCM considers the contribution of adjacent but disconnected fractures to grid block permeability, resulting in overestimated permeability, while

the proposed FCM with DFS algorithm reasonably ignores the contribution of disconnected fractures to grid block permeability. Thus, the FCM with DFS algorithm can more accurately describe the permeability spatial variability in DFN model.

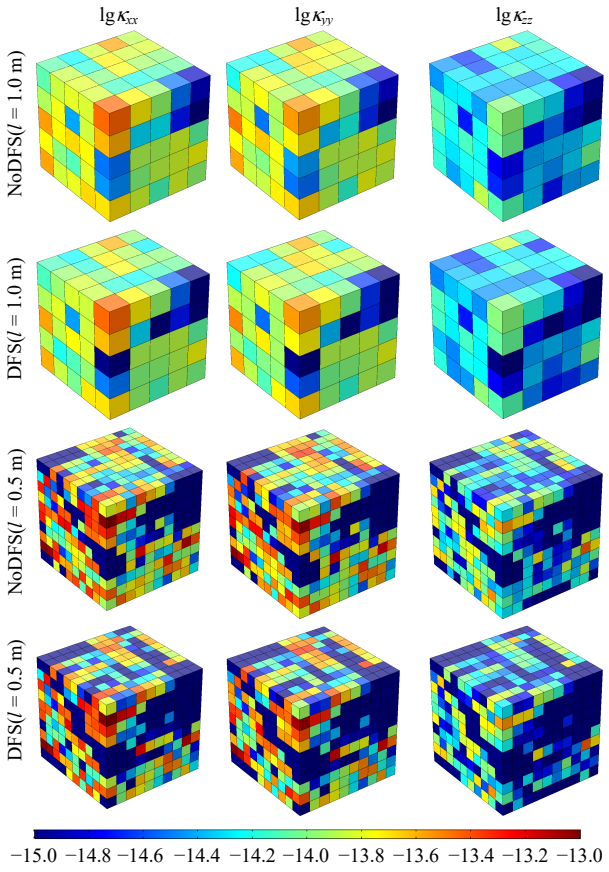

Fig. 11 Permeabilities in FCMs with and without DFS algorithm

5.2 Seepage and heat transfer simulation

Figure 12 compares the temperature fields in FCMs with and without DFS algorithm at 2×10^6 s. The low temperature range of the FCM without DFS algorithm is larger than that of the FCM with DFS algorithm under the same working condition. The grid blocks with exaggerated permeability in the conventional FCM leads to more low-temperature water flowing into the study domain, resulting in more extensive low-temperature area in fractured rock mass.

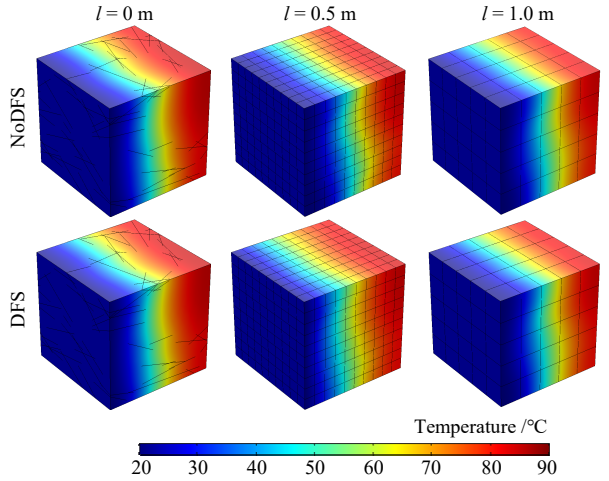

Fig. 12 Temperature fields in FCMs with and without DFS algorithm

6 Conclusions

To accurately and efficiently simulate the seepage and heat transfer processes in stochastic fractured rock mass, the existing 2D FCM is extended to 3D problems, which improves the theoretical research on the FCM for 3D seepage and heat transfer processes in stochastic fractured rock mass. The main conclusions are drawn as follows:

(1) The proposed FCM can simplify the 3D fractured rock mass, avoid the complex modeling and meshing of random discrete fractures, accurately describe the spatial variability of permeability, and accurately estimate the seepage flow and temperature field of stochastic fractured rock mass.

(2) Compared with the conventional FCM, the developed FCM combined with DFS algorithm can identify the adjacent but disconnected fractures, judge the connectivity between fractures and grid blocks, i.e. the seepage contribution of each fracture and hydraulic interactions between fractures can be considered. On the premise of reasonable grid block size, the seepage calculation accuracy of fractured rock mass with many minor fractures can be significantly improved based on the judgment of fracture connectivity.

(3) For the rock matrix with very low or high permeability, the effective DFN model can ensure the seepage accuracy. However, the relative error of the outflow calculated by the effective DFN model may exceed 5% for the rock matrix with moderate permeability, e.g. the ratio of rock matrix permeability to fracture permeability is in the range of 10^{-4}−10^{-6}.

In fact, the fracture surface of rock is undulating. The FCM is based on the parallel plate model to describe the fractures without considering tortuosity. This approximation may underestimate the heat transfer area between the fracture fluid and rock matrix. To better understand the seepage and heat transfer processes in fractured rock mass, the characteristics and connections of macro- and micro-scale physical processes of fracture will be further studied in the future work.

Declaration of competing interest

The authors declare that they have no known competing

financial interests or personal relationships that could have appeared to influence the work.

References

[1] ODA M. An Equivalent continuum model for coupled stress and fluid flow analysis in jointed rock masses[J]. Water Resources Research, 1986, 22(13): 1845−1856.

[2] ZIMMERMAN R W, CHEN G, HADGU T, BODVARSSON G S. A numerical dual-porosity model with semi-analytical treatment of fracture/matrix flow[J]. Water Resources Research, 1993, 29(7): 2127−2137.

[3] DVERSTORP B, ANDERSSON J. Application of the discrete fracture network concept with field data: possibilities of model calibration and validation[J]. Water Resources Research, 1989, 25(3): 540−550.

[4] NEUMAN S P. Trends, prospects and challenges in quantifying flow and transport through fractured rocks[J]. Hydrogeology Journal, 2005, 13(1): 124−147.

[5] CHEN T, CLAUSER C, MARQUART G, WILLBRAND K, et al. A new upscaling method for fractured porous media[J]. Advances in Water Resources, 2015, 80: 60−68.

[6] WANG M, CHEN Y F, MA G W, et al. Influence of surface roughness on nonlinear flow behaviors in 3D self-affine rough fractures: Lattice Boltzmann simulations[J]. Advances in Water Resources, 2016, 96: 373−388.

[7] SONG Xiao-chen, XU Wei-ya. A study on conceptual models of fluid flow in fractured rock[J]. Rock and Soil Mechanics, 2004, 25(2): 226−232.

[8] ASSTEERAWATT A. Flow and transport modelling of fractured aquifers based on a geostatistical approach[D]. Stuttgart: University of Universitätsbibliothek, 2008.

[9] BERRE I, DOSTER F, KEILEGAVLEN E. Flow in fractured porous media: a review of conceptual models and discretization approaches[J]. Transport in Porous Media, 2019, 130: 215−236.

[10] JIANG Zhong-ming, XIAO Zhe-zhen, TONG Dong, et al. Prediction of water inflow in water-sealed oil storage caverns based on fracture seepage effect[J]. Rock and Soil Mechanics, 2022, 43(4): 1041−1047, 1082.

[11] HOU Xiao-ping, FAN Heng-hui. Study on rainfall infiltration characteristics of unsaturated fractured soil based on COMSOL Multiphysics[J]. Rock and Soil Mechanics, 2022, 43(2): 563−572.

[12] EL A M F, AMIR S, SALAMA A, et al. Comparative study of shale-gas production using single−and dual−continuum approaches[J]. Journal of Petroleum Science and Engineering, 2017, 157: 894−905.

[13] VU M N, POUYA A, SEYEDI D M. Effective permeability of three−dimensional porous media containing anisotropic distributions of oriented elliptical disc−shaped fractures with uniform aperture[J]. Advances in Water Resources, 2018, 118: 1−11.

[14] HADGU T, KARRA S, KALININA E, et al. A comparative study of discrete fracture network and equivalent continuum models for simulating flow and transport in the far field of a hypothetical nuclear waste repository in crystalline host rock[J]. Journal of Hydrology, 2017, 553: 59−70.

[15] HARTLEY L, JOYCE S. Approaches and algorithms for groundwater flow modeling in support of site investigations and safety assessment of the Forsmark site, Sweden[J]. Journal of Hydrology, 2013, 500: 200−216.

[16] SWEETENHAM M G, MAXWELL R M, SANTI P M. Assessing the timing and magnitude of precipitation-induced seepage into tunnels bored through fractured rock[J]. Tunnelling and Underground Space Technology, 2017, 65: 62−75.

[17] SANDVE T H, BERRE I, NORDBOTTEN J M. An efficient multi−point flux approximation method for discrete fracture−matrix simulations[J]. Journal of Computational Physics, 2012, 231(9): 3784−3800.

[18] CHEN T, CLAUSER C, MARQUART G, et al. Upscaling permeability for three−dimensional fractured porous rocks with the multiple boundary method[J]. Hydrogeology Journal, 2018, 26(6): 1903−1916.

[19] LUO Shuang. Numerical analysis of coupled fluid flow and heat transfer at multiple scales in deep geothermal systems[D]. Beijing: Tsinghua University, 2018.

[20] LIU Chun-yan. The judgment of connected graph with adjacency matrix[J]. Journal of Jiamusi University (Natural Science Edition), 2012, 30(4): 592−594.